Biased Lévy Walk Enables Light Gradient Sensing in *Euglena gracilis*

Yu'an Li,[1,2] Yongfeng Zhao,[3,2] Siyuan Yang,[1,2] Min Tang,[2,4,*] and H. P. Zhang[1,2,†]
[1]*School of Physics and Astronomy, Shanghai Jiao Tong University, Shanghai 200240, China*
[2]*Institute of Natural Sciences and MOE-LSC, Shanghai Jiao Tong University, Shanghai 200240, China*
[3]*Center for Soft Condensed Matter Physics and Interdisciplinary Research and School of Physical Science and Technology, Soochow University, 215006 Suzhou, China*
[4]*School of Mathematics, Shanghai Jiao Tong University, Shanghai 200240, China*

(Received 24 June 2024; revised 1 November 2024; accepted 20 February 2025; published 13 March 2025)

We examine the navigation behavior of the photosensitive alga *Euglena gracilis* in confined environments. Under uniform lighting conditions, *E. gracilis* exhibits stochastic movements with nearly straight runs interrupted by abrupt directional changes. The lengths of these runs follow a long-tailed distribution typical of a Lévy walk, with scaling exponents that vary with light intensity. In gradient lighting conditions, the cells modulate their run durations—extending them upon detecting an increase in light intensity and shortening them when a decrease is detected. This adjustment effectively biases the Lévy walk, enabling the cells to ascend the spatial light gradient. This behavior mirrors well-known prokaryotic stochastic navigation strategies, such as bacterial chemotaxis, offering a eukaryotic parallel. The experimental observations under varied lighting conditions are consistently replicated through an agent-based model.

DOI: 10.1103/PhysRevLett.134.108301

Microorganisms, encompassing both prokaryotic and eukaryotic domains, have evolved diverse strategies to sense and respond to external cues such as chemical [1–9], light [10–22], gravitational [23,24], electrical fields [25,26], and fluid flow patterns [27,28]. Effective navigation is crucial for these organisms to adapt and flourish in natural environments, which are often marked by spatial heterogeneity and temporal fluctuations in resource availability [29–36]. Beyond their biological and ecological functions, investigations into these navigation strategies also have significant implications for theoretical and applied issues, such as optimal search strategies [37,38] and the control of biomimetic artificial microswimmers [36,39–41].

Prokaryotes, primarily archaea and bacteria, are characterized by their micrometric size, which limits their sensory capabilities and makes them susceptible to noise in signal detection. Consequently, prokaryotes often resort to stochastic navigation strategies. For example, bacteria bias the transition rates between run and tumble states to achieve chemotaxis [30,31,34,42–45]. In contrast, eukaryotic cells, such as algae and sperm, are larger and possess more sophisticated sensory systems and motility appendages, enabling them to use deterministic navigation strategies to traverse external fields [7,34]. For instance, these cells can adeptly sample chemical or light fields along their helical trajectories, adjusting their motility appendages based on sensory inputs to directly maneuver toward or away from stimuli [7–9,11,12,14,16,22].

In addition to deterministic behaviors, eukaryotic microorganisms also exhibit stochastic motion [9,46–49]. However, studies on eukaryotic stochastic motion remain limited, and it is unclear whether eukaryotic microorganisms can modulate their stochastic motion for navigation, as prokaryotic organisms do. To address this question, we examine the behavior of the photosensitive alga *Euglena gracilis* in a quasi-two-dimensional environment. Under uniform lighting, our experiments reveal "run-and-tumble" behavior, with run lengths exhibiting a long-tail distribution, indicative of a Lévy walk [38,50–63]. Upon exposure to a gradient light field, the cells adjust their run length in response to detected changes in light intensity, thereby biasing the Lévy walk to facilitate movement up the spatial gradient. Experimental findings are consistently replicated within an agent-based model with experimentally determined parameters. Our work suggests that modulating stochastic motion may represent a widespread navigational strategy employed by eukaryotic microorganisms.

Experiments—E. gracilis are single-celled, flagellated microorganisms characterized by their rod-shaped bodies, measuring approximately 50 μm in length and 5 μm in width. Propulsion and navigation are facilitated by a single flagellum, beating at frequencies ranging from 20 to 40 Hz [17,23,64]. Typically, *E. gracilis* swim directionally along their long axis at average speed of 70 μm/s, with a rotational motion around this axis occurring at a frequency of 1 Hz [20,65,66]. The presence of a photoreceptor enables

*Contact author: tangmin@sjtu.edu.cn
†Contact author: hepeng_zhang@sjtu.edu.cn

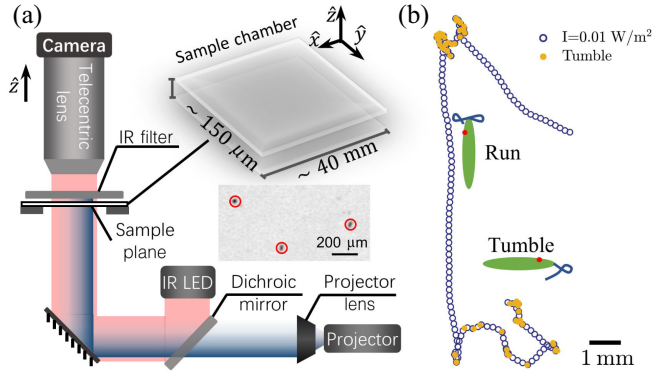

FIG. 1. (a) Schematic of the experimental setup with labeled parts. Inset: dimensions of the sample chamber (not to scale) and a segment from a raw experimental image, with three cells highlighted by red circles. See Fig. S1 for images of the setup. (b) Cell trajectory captured under low light condition, with tumble events denoted by filled yellow dots. Insets schematically show flagellum beating patterns at run and tumble states [17].

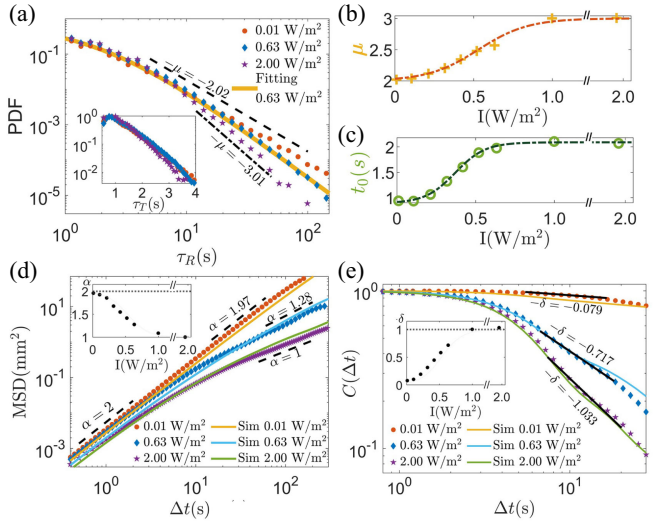

FIG. 2. Statistics of *E. gracilis* motion in uniform light fields. (a) Probability density function (PDF) of run-time τ_R under three light conditions. The yellow line represents the Lomax fitting [Eq. (1)] to data obtained with $I = 0.63$ W/m^2, where $\mu = 2.57$. Additional data and fittings are presented in Fig. S12. The inset displays the PDF of tumbling time τ_T under three light conditions. (b),(c) Lomax distribution exponent μ and the characteristic time t_0 as a function of light intensity. Empirical fits with a hyperbolic tangent function are represented by dash lines: $\mu(I) = 0.5\tanh(3.16(I-0.52)) + 0.25$, $t_0(I) = 0.6\tanh(5.27(I-0.37)) + 1.49$, where I and t_0 are expressed in units of W/m^2 and s, respectively. (d) Mean square displacement under three light conditions. The inset illustrates the intensity dependence of α parameters. (e) Velocity autocorrelation function under three light conditions. The inset demonstrates the intensity dependence of δ parameters. In (d) and (e), predictions of the agent-based model are represented by solid lines.

E. gracilis to perceive ambient light, thus modulating flagellar beating patterns to elicit various photo-responsive movements [14,17,64,67–72].

In our experiment setup, *E. gracilis* move in a quasi-two-dimensional chamber [17,20] measuring 40 mm × 40 mm × 150 μm, as depicted in Fig. 1(a). Cell motion is modulated by a pattern of blue light projected into the chamber, while uniform infrared illumination minimizes disruption to cell motility. A telecentric lens system offers an expansive field of view of 40 × 40 mm and a depth of field extending to 2 mm, coupled with a 16.8-megapixel camera for high-resolution capture of individual cells across the sample volume. Close-up images in the inset of Fig. 1(a) highlight the system's capability to capture detailed cellular motion, facilitating precise tracking of cell movements within the sample chamber over a wide dynamic range across spatial scales (10 μm to 40 mm) and temporal domains (1/10 to 10 000 s). Our experiments are conducted with low light intensities and small spatial gradients and cells do not exhibit phototaxis [14], photoshock behaviors [73], or polygonal and spin motilities [17] (Sec. I(G) in Supplemental Material (SM) [74]).

Lévy statistics in uniform light field—Our study begins by examining the motion of *E. gracilis* within uniform light fields for 25 min. Illustrated by Fig. 1(b) and detailed in Movie S1, cells exhibit two distinct phases: "runs," where cells move in a near-ballistic manner, and "tumbles," where they spin before selecting a new direction. This spontaneous switching behavior parallels observations in bacteria [4] and *Chlamydomonas* [47], where these phases were discerned by analyzing time series of cell translation and rotation speeds, as outlined in Sec. I(E) in SM.

We identify approximately 10^5 tumble events from cell trajectories under each uniform light condition. Subsequently, durations for each "run" and "tumble" phase, denoted as τ_R and τ_T, respectively, are quantified and used to construct probability distribution functions (PDFs) $P_R(\tau_R)$ and $P_T(\tau_T)$. Unlike the exponential distributions observed in *Chlamydomonas* [47], the run times in our experiments follows the Lomax distribution [38,42,83],

$$P_R(\tau_R, I) = \frac{1}{t_0(I)} \frac{\mu(I) - 1}{(1 + \tau_R/t_0(I))^{\mu(I)}}, \tag{1}$$

where $t_0(I)$ is a characteristic time, $\mu(I)$ is a scaling exponent, and I stands for the light intensity in units of W/m^2. Fits of the Lomax distribution to $P_R(\tau_R)$ are shown in Figs. 2(a) and S12. For τ_R larger than a few seconds [$\sim t_0(I)$], the run-time distributions have a long tail $P_R(\tau_R, I) \sim \tau_R^{-\mu(I)}, \mu(I) \in (2, 3)$, suggesting a Lévy walk mechanism [38]. We use individual cell trajectories [56], Akaike information criterion tests [52], and likelihood ratio tests [84,85] to show that the long-tail behavior is robust and arises from an inherent Lévy walk pattern (Sec. II(A) in SM). As depicted in Fig. 2(b), the power-exponent parameter μ decreases from 3 to 2 when the light intensity

decreases. This indicates that cells execute more long runs and tumble less frequently under dim light, as shown in Fig. S3 and Movie S1. Meanwhile, $t_0(I)$ in Fig. 2(c) increases from 1 to 2 s when the light intensity increases. The inset in Fig. 2(a) reveals that the PDF of tumble times obeys an exponential distribution with a mean tumble time $\bar{\tau}_T \sim 1.8$ s under all light conditions,

$$P_T(\tau_T) = \frac{1}{\bar{\tau}_T}\exp(-\tau_T/\bar{\tau}_T). \tag{2}$$

Furthermore, we characterize cell dynamics with mean square displacement (MSD). As shown in Fig. 2(d), MSD is ballistic (Δt^2) for small lag times Δt under all light conditions and shows different scaling for large lag times, Δt^α. The inset of Fig. 2(d) shows that cell motion is diffusive under strong blue light: $\alpha \approx 1$ for $I = 2$ W/m^2, and superdiffusive under other conditions. Summing the μ parameter from the run-time distribution with α, we find $\alpha + \mu \approx 4$ for all light conditions, consistent with the prediction of the Lévy walks theory [38]. We also check the individual cell's MSD and relation between α and μ to show that under a light intensity of 0.4 W/m^2 single alga exhibit superdiffusion and $\alpha + \mu \approx 4$ holds [Figs. S10(a), (b) and Sec. II in SM). Additionally, we compute velocity autocorrelation as $C(\Delta t) \equiv \langle \boldsymbol{v}(t) \cdot \boldsymbol{v}(t + \Delta t)\rangle / \langle \boldsymbol{v} \cdot \boldsymbol{v}\rangle$. As shown in Fig. 2(e), correlation function $C(\Delta t)$ decays as $\Delta t^{-\delta}$ for large Δt. The exponent δ is approximately related to α from MSD measurements as $\delta \approx 2 - \alpha$ [38].

Biased Lévy walk in gradient light fields—We begin by observing cell motion in a light field with intensity linearly increasing across the space. Figure 3(a) shows a typical cell trajectory in such a field, spanning 1700 s and consisting of run and tumble phases. To analyze the impact of the light gradient, we compute the angle (ϕ) between each run's displacement and the light gradient direction, as shown in the inset of Fig. 3(a). We sort all runs according to the ϕ values and compute the mean run-time $\bar{\tau}_R(\phi)$ for all runs in the same direction ϕ. Figure 3(b) reveals an anisotropic distribution and the mean run-time is approximately 30% longer (2 s) for $\phi \in (-\pi/4, \pi/4)$ compared to $\phi \in (3\pi/4, 5\pi/4)$. Similarly, we construct PDFs for run-time τ_R and observe the same long-tail exponent μ in PDFs for runs at different directions ϕ, as shown in Fig. 3(c). The inset of this figure confirms that tumble times follow the same exponential distribution seen in uniform fields. Additionally, Fig. S20(a) illustrates that the cell's mean speed is independent of ϕ, signifying the absence of photokinesis effects [14]. Figure 3(b) indicates that cells extend their runs when moving along the gradient, thus migrating from darker to brighter areas.

To further investigate stochastic navigation, we conduct experiments with a population of cells under both one-dimensional [Fig. 4(a)] and radial [Fig. 4(b)] blue-light gradient patterns, where light intensity varies from 0.05 to 0.35 or 0.45 W/m^2 along the horizontal (a) and radial (b) directions, respectively. Prior to the experiments, we allow the sample chamber to acclimate in the dark environment for several minutes, ensuring a uniform distribution of cells. Once the light pattern is activated, as depicted in Movies S2 and S3, cells migrate toward the brighter regions and attain a stable distribution within approximately 20 min. The stable distributions are shown in Figs. 4(a) and 4(b).

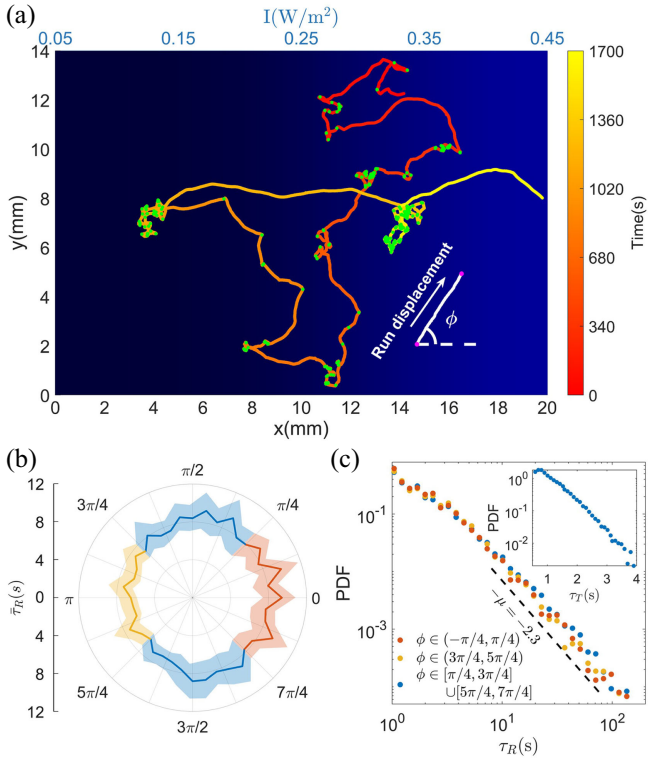

FIG. 3. Cell motion in a gradient light field. (a) Trajectory of an *E. gracilis* cell, with tumble events marked by green dots. The light intensity changes linearly from 0.05 W/m^2 (left) to 0.45 W/m^2 (right). The angle between the displacement of each run and the light gradient direction is denoted as ϕ in inset. (b) Dependence of the mean run-time, $\bar{\tau}_R(\phi)$, on the direction angle ϕ. Shading represents the 95% confidence intervals. Mean run-times for distinct angular regions are as follows: 8.5 s for up-gradient runs, 6.8 s for down-gradient runs, and 7.9 s for other angles. The event counts for the run-time statistics are approximately 6×10^3 for each of the up and down gradients. (c) Distributions of run-times for different motion directions, ϕ. The inset shows the distribution of tumble times.

Agent-based model—We consider noninteracting point-like particles navigating in two dimensions, alternating between persistent runs and finite-duration tumbles. During the run phase, each particle self-propels at a constant speed v, moving in a direction defined by an angle θ_i according to the equation

$$\dot{\boldsymbol{r}}_i = v\boldsymbol{e}(\theta_i), \tag{3}$$

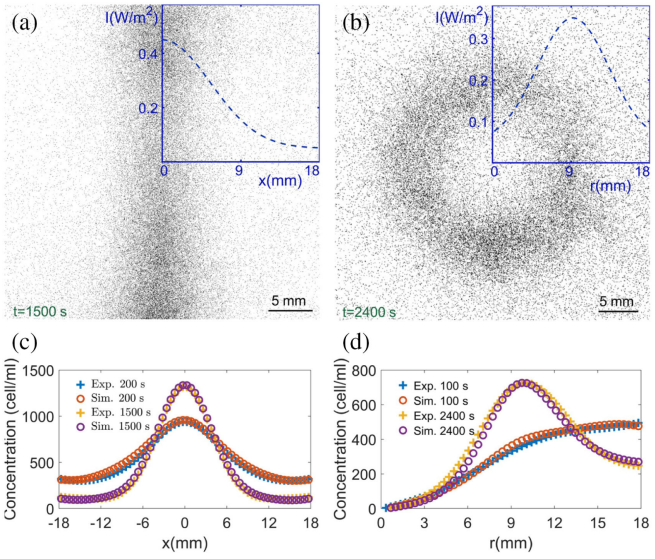

FIG. 4. Experimental and model results of cell distribution in gradient fields. (a) Steady-state cell distribution in a 1D Gaussian light field. (b) Steady-state cell distribution in a radial Gaussian light field. (c) Cell distributions at 200 s and 1500 s for 1D Gaussian pattern. (d) Cell distributions at 100 s and 2400 s for radial Gaussian field. Experimental data and agent-based model prediction in (c),(d) are shown by plus signs and circles, respectively. Light intensity profiles are shown in the insets of (a) and (b).

where $\boldsymbol{e}(\theta) = (\cos\theta, \sin\theta)$ is a unit vector in the direction of motion and v is set to the mean speed observed in the experiments (Fig. S5). The direction of motion θ_i changes during tumbles, when particles temporarily stop and randomly select a new θ_i from a uniform distribution on $(0, 2\pi)$ for the next run (Fig. S18).

To complete the model, we need to prescribe the PDFs of the run and tumble times. For uniform fields, experimentally measured distributions, $P_R(\tau_R)$ in Eq. (1) and $P_T(\tau_T)$ in Eq. (2), can be used directly with parameters $\mu = \mu(I)$ and $t_0 = t_0(I)$ described by tanh functions [Figs. 2(b) and 2(c)]. With these experimentally determined parameters, our model successfully reproduced the measured MSDs [Fig. 2(d)] and velocity correlation functions [Fig. 2(e)].

In gradient fields, Fig. 3(b) shows that the mean running time varies with the direction of cell movement with respect to the gradient. To incorporate this effect, we generalize $P_R(\tau_R)$ in Eq. (1) for a gradient field by assuming that cells measure the time derivative of light intensity along their trajectories in static light patterns: $\dot{I}(\boldsymbol{r}_i(t)) \approx v\boldsymbol{e}(\theta_i) \cdot \nabla I$ and increase or decrease run-time if $\dot{I}(\boldsymbol{r}_i(t))$ is positive or negative, respectively [2,3]. Given that the μ parameter in Eq. (1) does not depend on run direction [Fig. 3(c)], we replace the characteristic time $t_0(I)$ with $t_0'(I, \nabla I, \theta_i)$ as follows [3]:

$$t_0'(I, \nabla I, \theta_i) = t_0(I)\left[1 + \chi \tanh(\zeta v \boldsymbol{e}(\theta_i) \cdot \nabla I / I)\right], \quad (4)$$

where ζ controls the timescale of the sensed changes in light intensity, and χ is the sensitivity parameter. The full expression for the PDF of run-time τ_R is provided in Eq. (S6).

The agent-based model has two free parameters, ζ and χ in Eq. (4). To determine ζ and χ, we conduct simulations emulating the experimental conditions depicted in Fig. 4(a), employing the 1D Gaussian light pattern. Through an iterative process, we find that $\chi = 0.44$ and $\zeta = 150$ s yield the closest agreement between the model's predictions of cell density evolution and the experimental data [Figs. 4(c) and S22(a)]. With the determined ζ and χ parameters, we simulate the model in both radial [Fig. 4(b)] and linear [Fig. 3(a)] fields. The simulations accurately replicate the observed cell density dynamics in the radial field [Figs. 4(d) and S22(b)], without requiring any additional free parameters. Furthermore, Fig. S23 confirms that the model faithfully reproduces both the probability density function (PDF) of run-times and the angular distribution of mean run-times as observed in the linear gradient experiments.

Discussion—Through experiments [86] and biochemical calculations [87], researchers have determined the light detection threshold of *E. gracilis* to be approximately 0.05 W/m^2. Our experimental results support this estimation. As shown in Figs. 2(b) and 2(c), parameters (μ, t_0) in $P_R(\tau_R)$ display consistent values at two lowest light intensities (0.01 and 0.1 W/m^2) before rising sharply with increasing light intensity. This pattern indicates that these two lowest intensities are either below or near the detection threshold. The observation that *E. gracilis* exhibits Lévy walk behavior in dark environments with minimal detectable light suggests that the long-tailed distribution of run-times is not dependent on external stimuli and may instead arise from spontaneous fluctuations in cyclic adenosine monophosphate concentration, which is believed to regulate flagellar activity within the cellular signaling pathway [14,63,88,89].

MSDs in Fig. 2(d) show that long-time cell motion shifts from ballistic to diffusive regimes as the ambient light intensity increases. This shift in movement patterns from superdiffusion to diffusion occurs in response to varying resource availability (light, in this case). In environments where resources are sparse or patchily distributed, Lévy walks enable organisms to explore large areas quickly without frequently revisiting the same locations, thereby increasing the likelihood of encountering resources [51,55]. The long-tailed distribution of run-times also affects cellular transport in a flow [42,90] or near surfaces [44].

Tactic behavior has traditionally been modeled by continuum equations, with the Keller-Segel models serving as a notable example [91–95]. This motivates us to establish a connection between our agent-based model with continuum equations. As detailed in Sec. IV in SM, we derive a 1D fractional Keller-Segel equation [96–100] from the agent-based model.

Our experimental and computational modeling results provide compelling evidence for the biased random walk strategy employed by *E. gracilis*. This strategy may also be applicable to other eukaryotic microorganisms in which stochastic transitions between motion states have been observed [9,46–49]. In conjunction with prior research [30,34], our findings suggest that the biased random walk could be a widespread stochastic navigation strategy across both prokaryotic and eukaryotic microorganisms, despite their differences in sensory and motility systems. The strategy's versatility is further evidenced by its ability to guide run and tumble particles following either diffusive or Lévy statistics. These advantageous features also underscore its potential for developing control mechanisms in biomimetic artificial microswimmers.

Acknowledgments—We thank Hugues Chaté, Xia-qing Shi, Zijie Qu, and Quan-xing Liu for helpful discussions. This work was supported by the Ministry of Science and Technology Most China (No. 2021YFA0910700), the National Natural Science Foundation of China (No. 12225410, No. 12074243, No. 12304252, and No. 12031013). Y. Z. acknowledges support from the start-up funding of Soochow University.

[1] H. C. Berg and D. A. Brown, Nature (London) **239**, 500 (1972).
[2] T. S. Shimizu, Y. Tu, and H. C. Berg, Mol. Syst. Biol. **6**, 382 (2010).
[3] J. Saragosti, V. Calvez, N. Bournaveas, B. Perthame, A. Buguin, and P. Silberzan, Proc. Natl. Acad. Sci. U.S.A. **108**, 16235 (2011).
[4] J. B. Masson, G. Voisinne, J. Wong-Ng, A. Celani, and M. Vergassola, Proc. Natl. Acad. Sci. U.S.A. **109**, 1802 (2012).
[5] B. M. Friedrich and F. Julicher, Proc. Natl. Acad. Sci. U.S.A. **104**, 13256 (2007).
[6] K. F. Swaney, C.-H. Huang, and P. N. Devreotes, Annu. Rev. Biophys. Biomol. Struct. **39**, 265 (2010).
[7] L. Alvarez, B. M. Friedrich, G. Gompper, and U. B. Kaupp, Trends Cell Biol. **24**, 198 (2014).
[8] J. F. Jikeli, L. Alvarez, B. M. Friedrich, L. G. Wilson, R. Pascal, R. Colin, M. Pichlo, A. Rennhack, C. Brenker, and U. B. Kaupp, Nat. Commun. **6**, 7985 (2015).
[9] M. Zaferani and A. Abbaspourrad, Phys. Rev. Lett. **130**, 248401 (2023).
[10] L. Kuznicki, E. Mikołajczyk, P. L. Walne, and E. Hildebrand, Crit. Rev. Plant Sci. **9**, 343 (2008).
[11] G. Jekely, J. Colombelli, H. Hausen, K. Guy, E. Stelzer, F. Nedelec, and D. Arendt, Nature (London) **456**, 395 (2008).
[12] K. Drescher, R. E. Goldstein, and I. Tuval, Proc. Natl. Acad. Sci. U.S.A. **107**, 11171 (2010).
[13] A. Giometto, F. Altermatt, A. Maritan, R. Stocker, and A. Rinaldo, Proc. Natl. Acad. Sci. U.S.A. **112**, 7045 (2015).
[14] D.-P. Häder and M. Iseki, Photomovement in Euglena, in *Euglena: Biochemistry, Cell and Molecular Biology*, edited by S. D. Schwartzbach and S. Shigeoka (Springer International Publishing, Cham, 2017), Vol. 979, pp. 207–235.
[15] J. Dervaux, M. Capellazzi Resta, and P. Brunet, Nat. Phys. **13**, 306 (2016).
[16] J. Arrieta, A. Barreira, M. Chioccioli, M. Polin, and I. Tuval, Sci. Rep. **7**, 3447 (2017).
[17] A. C. H. Tsang, A. T. Lam, and I. H. Riedel-Kruse, Nat. Phys. **14**, 1216 (2018).
[18] T. Perlova, M. Gruebele, and Y. R. Chemla, J. Bacteriol. **201**, e00762 (2019).
[19] H. de Maleprade, F. Moisy, T. Ishikawa, and R. E. Goldstein, Phys. Rev. E **101**, 022416 (2020).
[20] S. Yang, M. Huang, Y. Zhao, and H. P. Zhang, Phys. Rev. Lett. **126**, 058001 (2021).
[21] A. Ramamonjy, J. Dervaux, and P. Brunet, Phys. Rev. Lett. **128**, 258101 (2022).
[22] K. C. Leptos, M. Chioccioli, S. Furlan, A. I. Pesci, and R. E. Goldstein, Phys. Rev. E **107**, 014404 (2023).
[23] D.-P. Häder and R. Hemmersbach, Gravitaxis in Euglena, in *Euglena: Biochemistry, Cell and Molecular Biology*, edited by S. D. Schwartzbach and S. Shigeoka (Springer International Publishing, Cham, 2017), Vol. 979, pp. 237–266.
[24] A. Sengupta, F. Carrara, and R. Stocker, Nature (London) **543**, 555 (2017).
[25] K. M. Nichols and R. Rikmenspoel, J. Cell Sci. **23**, 211 (1977).
[26] I. Elices, A. Kulkarni, N. Escoubet, L.-L. Pontani, A. M. Prevost, and R. Brette, PLoS Comput. Biol. **19**, e1010899 (2023).
[27] M. Zaferani, S. H. Cheong, and A. Abbaspourrad, Proc. Natl. Acad. Sci. U.S.A. **115**, 8272 (2018).
[28] T. Ohmura, Y. Nishigami, A. Taniguchi, S. Nonaka, T. Ishikawa, and M. Ichikawa, Sci. Adv. **7**, eabi5878 (2021).
[29] D. B. Dusenbery, *Sensory Ecology: How Organisms Acquire and Respond to Information* (W.H. Freeman, New York, 1992).
[30] H. C. Berg, *Random Walks in Biology* (Princeton University Press, Princeton, NJ, 2018).
[31] G. H. Wadhams and J. P. Armitage, Nat. Rev. Mol. Cell Biol. **5**, 1024 (2004).
[32] R. Stocker, Science **338**, 628 (2012).
[33] R. E. Goldstein, Annu. Rev. Fluid Mech. **47**, 343 (2015).
[34] K. Y. Wan and G. Jekely, Phil. Trans. R. Soc. B **376**, 20190758 (2021).
[35] J. M. Keegstra, F. Carrara, and R. Stocker, Nat. Rev. Microbiol. **20**, 491 (2022).
[36] F. Ji, Y. Wu, M. Pumera, and L. Zhang, Adv. Mater. **35**, 2203959 (2022).
[37] O. Bénichou, C. Loverdo, M. Moreau, and R. Voituriez, Rev. Mod. Phys. **83**, 81 (2011).
[38] V. Zaburdaev, S. Denisov, and J. Klafter, Rev. Mod. Phys. **87**, 483 (2015).
[39] Y. Hong, N. M. K. Blackman, N. D. Kopp, A. Sen, and D. Velegol, Phys. Rev. Lett. **99**, 178103 (2007).
[40] B. Dai, J. Wang, Z. Xiong, X. Zhan, W. Dai, C.-C. Li, S.-P. Feng, and J. Tang, Nat. Nanotechnol. **11**, 1087 (2016).
[41] J. Shao, M. Xuan, H. Zhang, X. Lin, Z. Wu, and Q. He, Angew. Chem. Int. Ed. **56**, 12935 (2017).

[42] N. Figueroa-Morales, A. Rivera, R. Soto, A. Lindner, E. Altshuler, and E. Clement, Sci. Adv. **6**, eaay0155 (2020).
[43] N. Figueroa-Morales, R. Soto, G. Junot, T. Darnige, C. Douarche, V. A. Martinez, A. Lindner, and É. Clément, Phys. Rev. X **10**, 021004 (2020).
[44] G. Junot, T. Darnige, A. Lindner, V. A. Martinez, J. Arlt, A. Dawson, W. C. K. Poon, H. Auradou, and E. Clément, Phys. Rev. Lett. **128**, 248101 (2022).
[45] C. Kurzthaler, Y. Zhao, N. Zhou, J. Schwarz-Linek, C. Devailly, J. Arlt, J.-D. Huang, W. C. K. Poon, T. Franosch, J. Tailleur, and V. A. Martinez, Phys. Rev. Lett. **132**, 038302 (2024).
[46] K. Y. Wan and R. E. Goldstein, Phys. Rev. Lett. **121**, 058103 (2018).
[47] M. Polin, I. Tuval, K. Drescher, J. P. Gollub, and R. E. Goldstein, Science **325**, 487 (2009).
[48] M. Huang, W. Hu, S. Yang, Q. X. Liu, and H. P. Zhang, Proc. Natl. Acad. Sci. U.S.A. **118**, e2100493118 (2021).
[49] S. A. Bentley, H. Laeverenz-Schlogelhofer, V. Anagnostidis, J. Cammann, M. G. Mazza, F. Gielen, and K. Y. Wan, eLife **11**, e76519 (2022).
[50] G. M. Viswanathan, V. Afanasyev, S. V. Buldyrev, E. J. Murphy, P. A. Prince, and H. E. Stanley, Nature (London) **381**, 413 (1996).
[51] F. Bartumeus, F. Peters, S. Pueyo, C. Marrase, and J. Catalan, Proc. Natl. Acad. Sci. U.S.A. **100**, 12771 (2003).
[52] A. M. Edwards, R. A. Phillips, N. W. Watkins, M. P. Freeman, E. J. Murphy, V. Afanasyev, S. V. Buldyrev, M. G. da Luz, E. P. Raposo, H. E. Stanley, and G. M. Viswanathan, Nature (London) **449**, 1044 (2007).
[53] D. W. Sims, E. J. Southall, N. E. Humphries, G. C. Hays, C. J. Bradshaw, J. W. Pitchford, A. James, M. Z. Ahmed, A. S. Brierley, M. A. Hindell, D. Morritt, M. K. Musyl, D. Righton, E. L. Shepard, V. J. Wearmouth, R. P. Wilson, M. J. Witt, and J. D. Metcalfe, Nature (London) **451**, 1098 (2008).
[54] G. M. Viswanathan, S. V. Buldyrev, S. Havlin, M. G. E. Da Luz, E. P. Raposo, and H. E. Stanley, Nature (London) **401**, 911 (1999).
[55] N. E. Humphries, N. Queiroz, J. R. Dyer, N. G. Pade, M. K. Musyl, K. M. Schaefer, D. W. Fuller, J. M. Brunnschweiler, T. K. Doyle, J. D. Houghton, G. C. Hays, C. S. Jones, L. R. Noble, V. J. Wearmouth, E. J. Southall, and D. W. Sims, Nature (London) **465**, 1066 (2010).
[56] S. Petrovskii, A. Mashanova, and V. A. Jansen, Proc. Natl. Acad. Sci. U.S.A. **108**, 8704 (2011).
[57] G. M. Viswanathan, M. G. E. da Luz, E. P. Raposo, and H. E. Stanley, *The Physics of Foraging: An Introduction to Random Searches and Biological Encounters* (Cambridge University Press, Cambridge, England, 2011).
[58] M. de Jager, F. J. Weissing, P. M. Herman, B. A. Nolet, and J. van de Koppel, Science **332**, 1551 (2011).
[59] T. H. Harris, E. J. Banigan, D. A. Christian, C. Konradt, E. D. Tait Wojno, K. Norose, E. H. Wilson, B. John, W. Weninger, A. D. Luster, A. J. Liu, and C. A. Hunter, Nature (London) **486**, 545 (2012).
[60] D. A. Raichlen, B. M. Wood, A. D. Gordon, A. Z. P. Mabulla, F. W. Marlowe, and H. Pontzer, Proc. Natl. Acad. Sci. U.S.A. **111**, 728 (2014).
[61] G. Ariel, A. Rabani, S. Benisty, J. D. Partridge, R. M. Harshey, and A. Be'er, Nat. Commun. **6**, 8396 (2015).
[62] A. M. Reynolds, Biol. Open **7**, bio030106 (2018).
[63] H. Huo, R. He, R. Zhang, and J. Yuan, Appl. Environ. Microbiol. **87**, e02429 (2021).
[64] B. Diehn, Science **181**, 1009 (1973).
[65] M. Rossi, G. Cicconofri, A. Beran, G. Noselli, and A. DeSimone, Proc. Natl. Acad. Sci. U.S.A. **114**, 13085 (2017).
[66] N. Giuliani, M. Rossi, G. Noselli, and A. DeSimone, Phys. Rev. E **103**, 023102 (2021).
[67] C. Creutz, G. Colombetti, and B. Diehn, Photochem. Photobiol. **27**, 611 (1978).
[68] D.-P. Hader, G. Colombetti, F. Lenci, and M. Quaglia, Arch. Microbiol. **130**, 78 (1981).
[69] M. Iseki, S. Matsunaga, A. Murakami, K. Ohno, K. Shiga, K. Yoshida, M. Sugai, T. Takahashi, T. Hori, and M. Watanabe, Nature (London) **415**, 1047 (2002).
[70] K. Ozasa, J. Lee, S. Song, and M. Maeda, Plant Cell Physiol. **55**, 1704 (2014).
[71] T. Ogawa, E. Shoji, N. J. Suematsu, H. Nishimori, S. Izumi, A. Awazu, and M. Iima, PLoS One **11**, e0168114 (2016).
[72] K. Muku, H. Yamashita, T. Kamikubo, N. J. Suematsu, and M. Iima, Front. Cell Dev. Biol. **11**, 1133028 (2023).
[73] M. J. Doughty, J. Photochem. Photobiol., B **9**, 75 (1991).
[74] See Supplemental Material at http://link.aps.org/supplemental/10.1103/PhysRevLett.134.108301, which includes Refs. [75–82], detailed experimental and numerical procedures, additional experimental and numerical results, and movies from experiments.
[75] H. P. Zhang, A. Be'er, E.-L. Florin, and H. L. Swinney, Proc. Natl. Acad. Sci. U.S.A. **107**, 13626 (2010).
[76] M. Theves, J. Taktikos, V. Zaburdaev, H. Stark, and C. Beta, Biophys. J. **105**, 1915 (2013).
[77] H. Laeverenz-Schlogelhofe and K. Y. Wan, Curr. Biol. **34**, 697 (2024).
[78] K. Ozasa, J. Won, S. Song, T. Shinomura, and M. Mizuo, Algal. Res. **41**, 101563 (2019).
[79] D. Froemberg, M. Schmiedeberg, E. Barkai, and V. Zaburdaev, Phys. Rev. E **91**, 022131 (2015).
[80] L. Alessandretti, P. Sapiezynski, S. Lehmann, and A. Baronchelli, PLoS One **12**, e0171686 (2017).
[81] B. J. West, P. Grigolini, R. Metzler, and T. F. Nonnenmacher, Phys. Rev. E **55**, 99 (1997).
[82] M. H. DeGroot and M. J. Schervish, *Probability and Statistics* (Addison-Wesley, Boston, 2012).
[83] K. S. Lomax, J. Am. Stat. Assoc. **49**, 847 (1954).
[84] A. Clauset, C. R. Shalizi, and M. E. J. Newman, SIAM Rev. **51**, 661 (2009).
[85] J. Alstott, E. Bullmore, and D. Plenz, PLoS One **9**, e85777 (2014).
[86] H. Ooka, T. Ishii, K. Hashimoto, and R. Nakamura, RSC Adv. **4**, 20693 (2014).
[87] L. Barsanti and P. Gualtieri, Encyclopedia **4**, 26 (2024).
[88] Y. Tu and G. Grinstein, Phys. Rev. Lett. **94**, 208101 (2005).
[89] M. S. Abe, Proc. Natl. Acad. Sci. U.S.A. **117**, 24336 (2020).
[90] Z. Pasternak, F. Bartumeus, and F. W. Grasso, J. Phys. A **42**, 434010 (2009).

[91] E. F. Keller and L. A. Segel, J. Theor. Biol. **26**, 399 (1970).
[92] E. F. Keller and L. A. Segel, J. Theor. Biol. **30**, 225 (1971).
[93] T. Hillen and K. J. Painter, J. Math. Biol. **58**, 183 (2009).
[94] N. Bellomo, A. Bellouquid, Y. Tao, and M. Winkler, Math. Models Methods Appl. Sci. **25**, 1663 (2015).
[95] G. Arumugam and J. Tyagi, Acta Appl. Math. **171**, 6 (2021).
[96] G. Estrada-Rodriguez, H. Gimperlein, and K. J. Painter, SIAM J. Appl. Math. **78**, 1155 (2018).
[97] B. Perthame, W. Sun, and M. Tang, Z. Angew. Math. Phys. **69**, 67 (2018).
[98] X. Xue and M. Tang, J. Math. Biol. **83**, 27 (2021).
[99] T. Zhou, Z. Peng, M. Gulian, and J. F. Brady, J. Phys. A **54**, 275002 (2021).
[100] R. Stern, F. Effenberger, H. Fichtner, and T. Schäfer, Fract. Calc. Appl. Anal. **17**, 171 (2013).